



Evaluation of dynamic SIF during crack propagation in layered plates having property variation along the crack front

SERVESH KUMAR AGNIHOTRI

Department of Mechanical–Mechatronics Engineering, The LNM Institute of Information Technology (LNMIIT), Jaipur, Rajasthan, India
e-mail: servesh29@gmail.com

MS received 19 May 2019; revised 4 November 2019; accepted 3 March 2020; published online 25 May 2020

Abstract. The present study emphasizes understanding the crack propagation in layered structures under dynamic loading conditions when the property jumps occur across the crack front. Layered plates were made by joining polymethylmethacrylate (PMMA) and epoxy sheets using an epoxy-based adhesive (Araldite). Single edge notched (SEN) specimens were subjected to dynamic loading using a modified Hopkinson bar setup. An array of strain gauges installed on surfaces of specimen was used to record the strain history in the layers during crack propagation from which the dynamic stress intensity factor (SIF) during crack propagation was evaluated. Photographs of the propagating crack front were also simultaneously captured using a high-speed imaging camera to obtain the crack tip location history in each layer.

Keywords. Layered plates; dynamic stress intensity factors; strain gauge; impact.

1. Introduction

Layered structures are widely used in applications such as heavy armor, thermal protection systems, and windshields. Using layered materials, properties of individual layers can be controlled and required properties can be imparted to the overall structure. The fracture behavior of these structures is complex due to the presence of sharp interfaces in the structure.

Many previous authors have studied the fracture behavior of layered materials especially the bi-materials systems [1–13]. The dynamic behavior of cracks running either along the interface or across the interface has been investigated using the optical techniques such as photoelasticity, Moiré interferometry, caustics and coherent gradient sensing. These techniques when combined with fast-imaging techniques, gather detailed information about mechanical fields near the tip of a propagating crack. On the other hand, strain gauge methods have also been used to investigate fracture under dynamic loading conditions in various materials [14–16]. Subsequently the method of strain gauges has also been used in composite materials to investigate interfacial fracture under dynamic loading conditions [17–21]. Several numerical approaches have been also developed to treat the layered plate problem under dynamic loading [22–25]. In the existing studies of dynamic fracture of layered materials, crack propagation is either along the interface or across the interface and the properties are constant through the thickness of the crack front. However, very few studies are available in which elastic and fracture properties in a layered plate vary discretely through the thickness of the crack front [26, 27].

In recent years, layered plate having jumps in both elastic and fracture properties through the thickness of the crack front has received considerable attention. Bankar and Parameswaran [28] and Agnihotri and Parameswaran [29] examined respectively the mode-I (opening mode) fracture and mixed mode (mode-I and mode-II) fracture in epoxy–PMMA (E–P) and PMMA–epoxy–PMMA (P–E–P) layered plates subjected to in-plane bending. Recently, Agnihotri and Parameswaran [30] investigated the dynamic fracture of layered plates using single strain gauge and photoelasticity method. This study was limited to the evaluation of crack initiation toughness and crack propagation toughness in a lesser stiffness layer i.e., epoxy only. In this study, the same type of layered structures i.e., E–P and P–E–P is reexamined using three strain gauges on either side of the plate and the dynamic stress intensity factor (DSIF) histories during crack propagation have been evaluated for both the layers i.e. epoxy and PMMA. The layered system consisted of two different polymers: epoxy (LY556) and PMMA [28–30]. Dynamic SIF has been evaluated using the strain histories recorded during crack propagation and simultaneously crack propagation images were also captured using a high-speed camera. The details of the work are presented in section 2–4.

2. Experimental details

2.1 Specimen preparation

Single edge notched (SEN) specimens of size 225 mm × 50 mm were prepared by first joining epoxy sheets of size

250 mm × 75 mm × 5.8 mm and PMMA sheets of size 250 mm × 75 mm × 5.5 mm using an Araldite and then machined out to the required size (225 mm × 50 mm). Both sheets are transparent, allowing one to clearly observe the fracture path during crack propagation in either of the layer of the layered plate. PMMA sheets of nominal thickness 5.5 mm and 2.7 mm were commercially procured. Epoxy sheets of nominal thickness 5.8 mm were cast in-house. The details of the casting process of epoxy sheets and then bonding with PMMA sheets were reported in [28–30]. Plates were having two different configurations as shown in figure 1. In the first configuration, referred to as E–P plate, a single layer of epoxy was bonded to a single layer of PMMA. In the second configuration, referred to as P–E–P plate, a single layer of epoxy was sandwiched between the two layers of PMMA of nominal thickness 2.7 mm. Both configurations, therefore, had the same total thickness. In a layered plate, a notch was introduced using a saw, and a natural crack was lengthened by forcing a sharp razor blade into the root of the notch. The measured elastic, fracture and optical properties of epoxy and PMMA are given in table 1.

2.2 Experimental set up for dynamic fracture

An array of strain gauges was mounted at an obtuse angle and above the *x*-axis (crack line) of specimens, as shown in figure 1. As discussed in [31], strain gauges at an obtuse angle are much sensitive than the acute angle in providing the crack tip position from the strain profile. Six strain gauges, three on either side of the E–P plate, were mounted at an angle ($\beta = 121^\circ$) to the positive *x*-axis and located at a vertical distance of 6.93 mm from the *x*-axis and 4 mm apart from each other (figure 1). Specimens were tested at various loading rates. Crack length to width (*a/w*) ratio (0.3) was kept fixed for all experiments. A modified

Hopkinson bar setup shown in figure 2 was used to load the specimens. The set up consists of a loading bar and striker bar made of polycarbonate. The length and diameter of the loading bar were 3070 mm and 12.5 mm, respectively. The length of the striker bar was 395 mm. The real-time digital images of high-speed fracture process were recorded using SIM02-16 high-speed camera (specialized imaging Ltd., UK, max. framing rate – 200 × 10⁶fps, 1 MP fixed resolution) or photron camera (PHOTRON USA, INC.) based on the framing rate and image resolution requirements. The photron camera can be used with variable image resolution from 96 × 96 pixels (max. frame rate – 675,000 fps) to 1024 × 1024 pixels (max. frame rate – 5400 fps). The camera was oriented in such a way that the images of the crack growth in the layered plate can be easily visualized.

In experiments, the striker hits the bar and subsequently, the incident and reflected wave travels back and forth through the length of the bar after striking the specimen. The wave signals of the bar were recorded using the strain gauges mounted at the mid-length of the bar. The strain signals were conditioned using strain conditioner (Ectron 563) and recorded using a NI-PCI 6115 data acquisition card at a sampling rate of 1 MHz. The triggering sequence is indicated in figure 2 (i.e., Bar strain gauges to an oscilloscope to high-speed camera to data acquisition system).

After setting appropriate initial delay time, a set of images were captured by the camera at framing rates of 10⁵ fps or 1.5 × 10⁵ fps during the crack propagation in the layered plate. The xenon flash lamps used for illumination were slave triggered by the high-speed camera. Monitor signals from the camera were also recorded to synchronize the images with the Hopkinson bar signals.

2.3 Dynamic crack propagation toughness evaluation

A three-term representation of the strain field for a moving crack can be written as [31],

$$2\mu\epsilon_g = C_0f_0 + C_1f_1 + D_0g_0$$

$$f_0 = D \begin{cases} -1/2 \left[\rho_1 (\lambda_1^2 - \lambda_2^2) \cos \frac{\phi_1}{2} + (1 + \lambda_1^2) \cos 2\alpha \cos \frac{\phi_1}{2} + 2\lambda_1 \sin 2\alpha \sin \frac{\phi_1}{2} \right] \\ -\rho_2 \left[\frac{4\lambda_1\lambda_2}{1 + \lambda_2^2} \cos 2\alpha \cos \frac{\phi_2}{2} + 2\lambda_1 \sin 2\alpha \sin \frac{\phi_2}{2} \right] \end{cases}$$

$$f_1 = D \begin{cases} \rho_1^{1/2} \left[\kappa (\lambda_1^2 - \lambda_2^2) \cos \frac{\phi_1}{2} + (1 + \lambda_2^2) \cos 2\alpha \cos \frac{\phi_1}{2} - 2\lambda_1 \sin 2\alpha \sin \frac{\phi_1}{2} \right] \\ -\rho_2^{1/2} \left[\frac{4\lambda_1\lambda_2}{1 + \lambda_2^2} \cos 2\alpha \cos \frac{\phi_2}{2} - 2\lambda_1 \sin 2\alpha \sin \frac{\phi_2}{2} \right] \end{cases}$$

$$g_0 = D(\lambda_1^2 - \lambda_2^2)(\kappa + \cos 2\alpha)$$

(1)

where μ is shear modulus of the material, $D = \frac{1 + \lambda_2^2}{4\lambda_1\lambda_2 - (1 + \lambda_2^2)^2}$, $\lambda_1 = \sqrt{1 - \frac{c^2}{c_l^2}}$, $\lambda_2 = \sqrt{1 - \frac{c^2}{c_s^2}}$, *c* refers to the crack speed, *c_l* and *c_s* are the dilatational and shear wave speed in the material respectively and ρ is the density

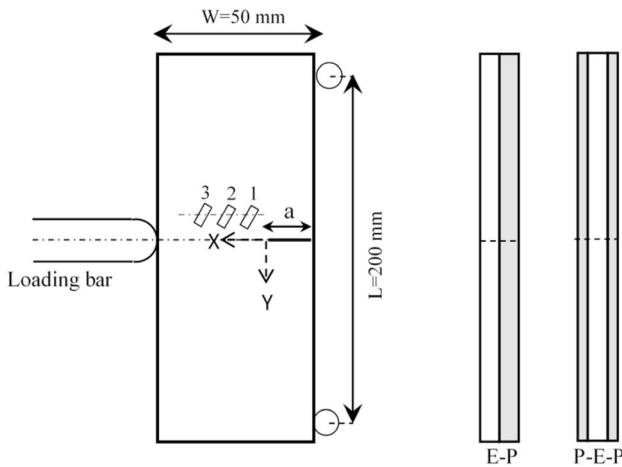


Figure 1. Three-point bend specimen geometry.

Table 1. Properties of materials used [30].

Material	Elastic Modulus (GPa)	Poisson's ratio	Fringe constant (MPa-m/fringe)	Fracture toughness (MPa-√m)	Dilatational wave speed (m/s)	Shear wave speed (m/s)
PMMA	2.67	0.34	0.240	0.95 ± 0.11	2630	1280
Epoxy	4.16	0.35	0.018	0.67 ± 0.09	2600	1220

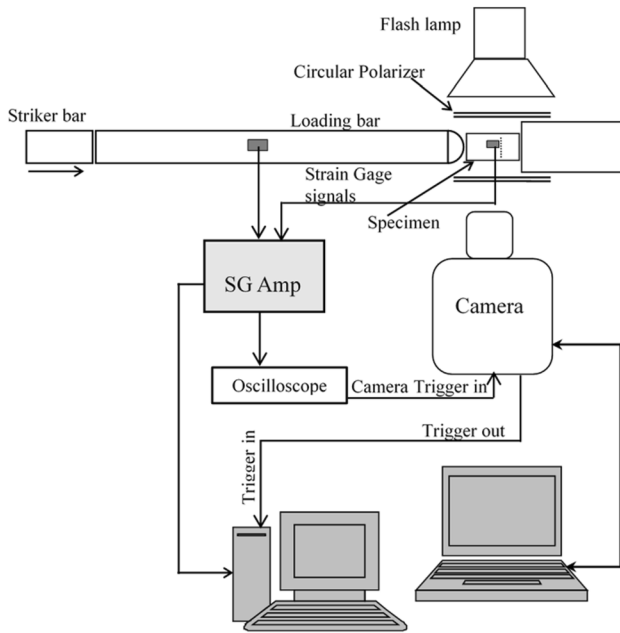


Figure 2. Modified Hopkinson bar set up.

of the material. ρ_1 and ρ_2 are $\sqrt{x^2 + (\lambda_1 y)^2}$ and $\sqrt{x^2 + (\lambda_2 y)^2}$ respectively. In Eq. (1), g_0 the term corresponding to D_0 will vanish if the gauge orientation is such that

$$\cos 2\alpha = -\kappa \tag{2}$$

Equation 2 provides two values of angle α for a given material; one will be an acute angle and the other obtuse angle. As discussed in [31], the choice of an obtuse angle provides definite signature for determining the crack tip location directly from the strain profile. In addition, gauge located at an obtuse angle provides better sensitivity than the acute angle. In the current study, an obtuse angle configuration was used to measure the peak strains when the crack tip is directly below the gauge. As shown in figure 1, six strain gauges, three on either side of the E–P plate, were oriented at an angle ($\alpha = 121^\circ$) to the positive x -axis and located at a vertical distance of 6.93 mm from the x -axis and 4 mm apart from each

other. In P–E–P plate, three strain gauges were installed on the PMMA surface.

For the considered configuration when the crack tip is directly below the gauge, the DSIF (K_{1D}) from the peak strain can be evaluated using Eq. (3) [31].

$$K_{1D} = \frac{4\mu}{D} (\varepsilon_g)_{peak} \sqrt{\pi y_g} \left\{ \frac{1}{\sqrt{\lambda_1}} [\kappa(\lambda_1^2 - \lambda_2^2) + (1 + \lambda_1^2) \cos 2\alpha + 2\lambda_1 \sin 2\alpha] \right\}^{-1} \left\{ -\frac{1}{\sqrt{\lambda_2}} \left[\frac{4\lambda_1 \lambda_2}{1 + \lambda_2^2} \cos 2\alpha + 2\lambda_1 \sin 2\alpha \right] \right\} \tag{3}$$

In deriving Eq. (3) from Eq. (1), only $r^{-1/2}$ term (corresponding to C_0) is considered to evaluate the DSIF and the effect of $r^{1/2}$ term (corresponding to C_1) is neglected. However, in most of the specimen geometry, the term corresponding to C_1 influences the magnitude of the peak strain and the spread of the strain signal and cannot be ignored to estimate the DSIF. A revised procedure similar to that employed by Sanford *et al* [15] is employed here to correct the estimation of DSIF. Equation 1 can be written in modified form as

$$\frac{2\mu\varepsilon_g}{C_0} = f_0 + \frac{C_1}{C_0} f_1 \tag{4}$$

For the chosen values of α (121°), the response of the gauge was obtained from Eq. (4). Figure 3 shows the modified strain ($2\mu\varepsilon_g/C_0$) as a function of position for selected values of (C_1/C_0). It can be observed that the peak value of strain strongly depends on C_1/C_0 ($\sim 40\%$). However, the position of the peak strain differs slightly from the gauge position except for $C_1 = 0$. From figure 3, the range of x (gauge position) or equivalent time duration for which the strain is greater than 75% of peak strain was extracted for different values of C_1/C_0 . A master curve was generated between equivalent time duration $(\Delta t)_{3/4}$ and different ratios of C_1/C_0 , as shown in figure 4. The $(\Delta t)_{3/4}$ corresponding to experimental strain signal was used to extract the ratio C_1/C_0 from the master curve. The ratio C_1/C_0 was used in Eq. (4) to determine the value of C_0 from which DSIF, $K_{1D} = C_0 \sqrt{2\pi}$ was estimated.

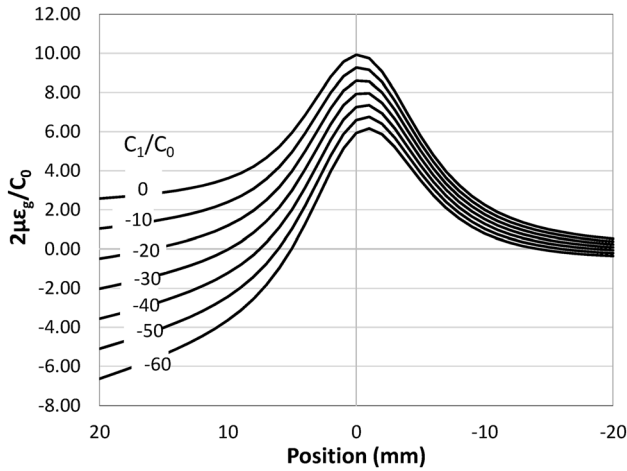


Figure 3. Modified strain as a function of position.

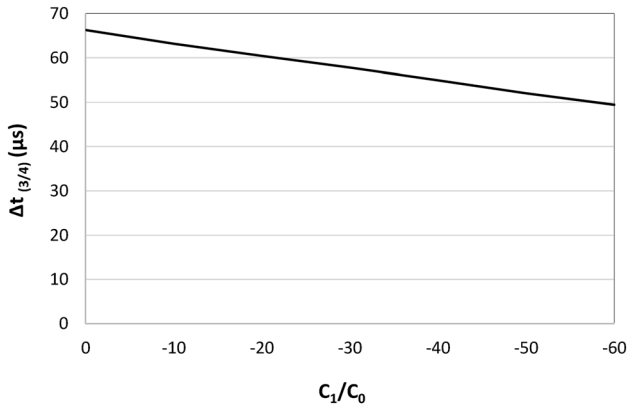


Figure 4. Time parameter $(\Delta t)_{3/4}$ versus coefficient ratio C_1/C_0 .

2.4 Determination of dynamic load point force and velocity

As shown in figure 2, two diametrically opposite strain gauges were installed at the mid-length of the loading bar to avoid the bending strains in the bar. Strain signal, recorded at mid length of bar, cannot be considered as experimental strain at the end of the bar due to dispersion and attenuation effects of wave propagation in viscoelastic material. Authors have investigated these effects and proposed several methods to correct the strain signal at the end of the bar [32–36]. In the current study, the method advised by Bacon [34] and implemented in Varshney [37] was used to calculate the experimental strain at the end of the bar. An impact test using a steel spherical projectile of 9 mm was performed and incident (ε_i) and reflected strains (ε_r) signals were recorded at the center of the bar. The transfer function $H(\omega)$ was then obtained as

$$H(\omega) = -\frac{\bar{\varepsilon}_r(\omega)}{\bar{\varepsilon}_i(\omega)} \quad (5)$$

where $\bar{\varepsilon}_i(\omega)$ and $\bar{\varepsilon}_r(\omega)$ are the Fourier transforms of ε_i and ε_r , respectively. Attenuation coefficient $\alpha(\omega)$ and phase velocity $c(\omega)$ were then calculated from the amplitude and phase of the transfer function following Bacon [34] as

$$\alpha(\omega) = -\frac{\log(\text{abs}(H(\omega)))}{2d} \quad (6)$$

and

$$c(\omega) = -\frac{2d\omega}{\arg(H(\omega))} \quad (7)$$

where d is the distance from the center to the end of the bar. The propagation coefficient was defined as $\gamma(\omega) = \alpha(\omega) + i\omega/c(\omega)$. Complex Young's modulus of the bar (ξ) is related to the propagation coefficient as

$$\xi = -\rho\omega^2/\gamma^2 \quad (8)$$

where, ρ is the density of polymeric bar. The propagation coefficient can be used to determine strain at any cross section from the knowledge of strain at some other location and the distance between two. A typical strain signals obtained in the experiment after dispersion correction is shown in figure 5. Significant attenuation in the strain signals can be noticed.

Force and velocity histories at the end of the bar are calculated as (Bacon 1999),

$$\bar{F}(d, \omega) = -\xi A_b [\varepsilon_i(\omega)e^{-\gamma d} + \varepsilon_r(\omega)e^{\gamma d}] \quad (9)$$

with $F(d, t) = F^{-1}(\bar{F}(d, \omega))$,

And

$$\bar{v}(d, \omega) = -i\omega/\gamma [\varepsilon_i(\omega)e^{-\gamma d} - \varepsilon_r(\omega)e^{\gamma d}] \quad (10)$$

with $v(d, t) = F^{-1}(\bar{v}(d, \omega))$.

3. Results and discussion

As reported in [30], the time delay between crack initiations in layered structures was affected by the impact velocity. Subsequently, the SIF gradient and speed of the propagating crack was also affected by the impact velocity. This requires the specimen has to be tested at different impact velocities. Dynamic fracture experiments were conducted at various loading rates by systematically varying the impact velocity of the bar from 1.75 to 7.33 m/s. These velocities were measured after firing the striker at different pressure (lower to higher) and are not specific, only ensuring the behavior reported in [30]. The strain histories recorded at the mid-length of the bar were analyzed to determine the force at the bar-specimen interface, as discussed in section 2.4. Figure 6 shows the variation of

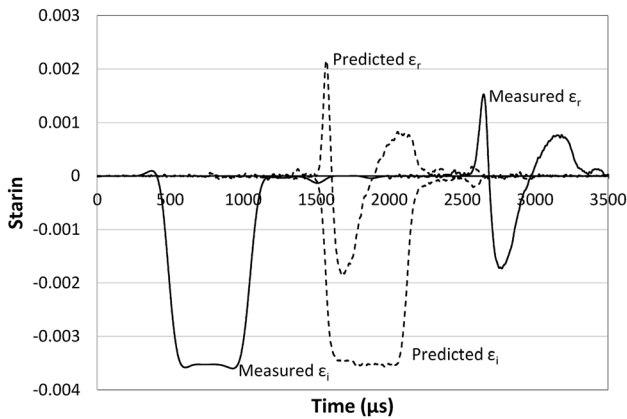


Figure 5. Predicted incident and reflected strains at the end of the bar.

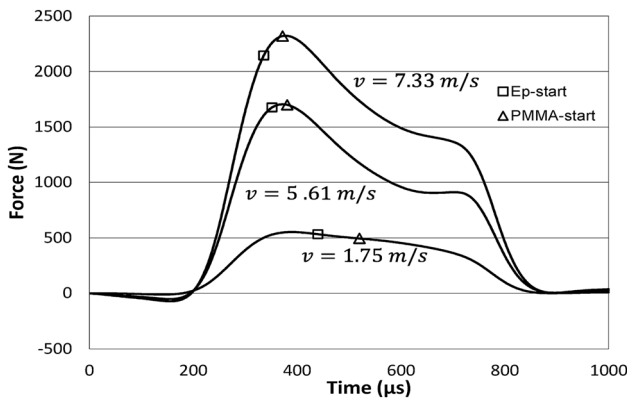


Figure 6. Variation of dynamic load-point force at different incident velocities.

dynamic load-point force at different impact velocities of bar. Square and triangle symbols indicate the epoxy and PMMA crack initiation respectively in E–P plate. It was observed that at low impact velocity (1.75 m/s) both epoxy and PMMA crack initiate after reaching the peak force. However, at high impact velocities (5.61 and 7.33 m/s), the cracks in both layers initiate just before reaching the peak force. Maximum load sustained by the specimens at various impact velocities was 553, 1700 and 2320 N.

Experiments were performed to track the crack growth in each layer by viewing the plate at an oblique angle. Dynamic fracture behavior of each layer in layered plate was investigated by measuring the strains on each surface of the plate. In the following subsections, experimental observations will be discussed.

3.1 Evaluation of dynamic SIF of epoxy–PMMA (E–P) layered plate

As discussed in section 2.2, an array of three strain gauges on either side of the layered plate was mounted at an obtuse

angle (figure 1) to evaluate the dynamic SIF under dynamic loading. The specimens were tested at two different impact velocities and corresponding strain histories are shown in figure 7. As the specimen was impacted by the loading bar, stress waves travel back and forth in the specimen and load the crack tip in the layered structure. This increases the strain on both sides (epoxy and PMMA) of the layered plate. Once the crack starts propagating, the strain starts decreasing with time due to change in stiffness of the material. The time axis in figure 7 indicates the time of instantaneous crack tip position. Simultaneously the images of the crack growth were also captured using Photron camera. Crack lengths when the crack tip in each layer is just above the strain gauge locations are measured and plotted in figure 7. It can be noticed that strain in each layer reaches maximum when the crack in each layer traverses each gauge location. Figure 8 shows the stages of crack growth in epoxy–PMMA layered plate at an impact velocity of 1.75 m/s. Vertical line indicates the crack tip position in epoxy layer and arrow indicates the crack tip position in PMMA layer. The images were captured at a time interval of 10 μs. In image #1 crack tips in both epoxy

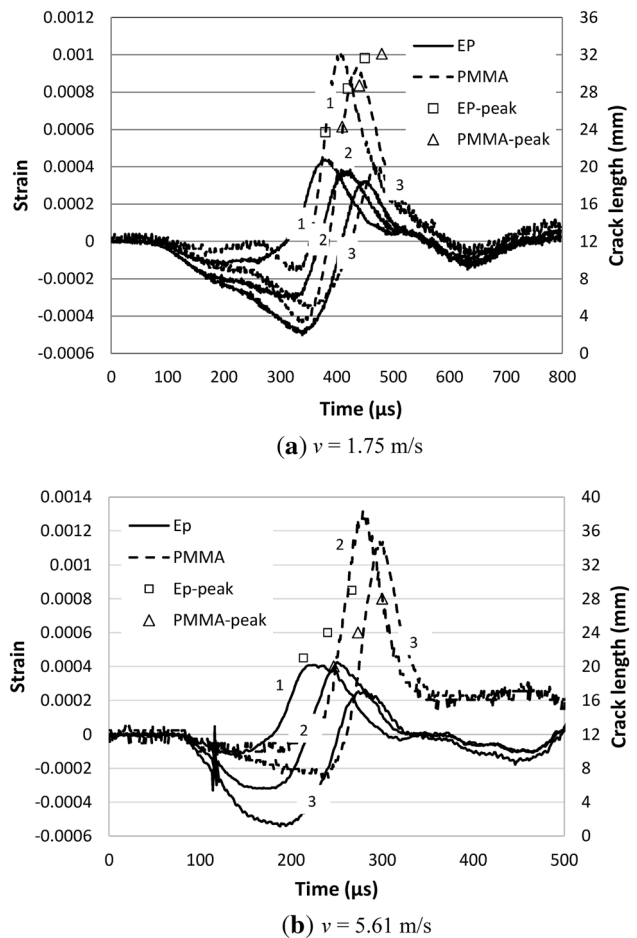


Figure 7. Strain histories in the E–P plate during crack propagation at various loading rates.

and PMMA layer are at the same location. Image #2 and #3 corresponds to the instant at which the crack in epoxy and PMMA layer extends respectively. Image #4, #5 and #6 corresponds to the instant at which the crack tips in epoxy layer are just above the strain gauge locations. From images #2 and #3, it can be noticed that the crack in epoxy layer initiates first then followed by the crack in PMMA layer. The delay in crack initiation in PMMA layer after the crack extension in epoxy layer was observed to be 80–90 μs . It can be observed that the crack front in epoxy layer is not straight. Crack advances more near the interior of the plate compared to locations near the interface. Crack advances less near the interface due to the closing traction applied by the un-cracked portion of the PMMA plate, resulting in an asymmetric crack front profile. Similarly images were also captured for an impact velocity of 5.61 m/s and 7.33 m/s at an inter-frame timing of 7 μs and subsequently delay in the crack extension in PMMA layer was observed to be 40 μs and 13 μs respectively.

As discussed in section 2.2, the equivalent time duration $(\Delta t)_{3/4}$ from each strain signal and corresponding C_1/C_0 ratio from figure 5 is extracted and reported in table 2. Crack in each layer extends through a series of jump and

arrest which affects the spreading of the strain signal and subsequently $(\Delta t)_{3/4}$ of each strain signal. In addition, this ratio is affected by the impact velocity of the bar. At high impact velocity, $(\Delta t)_{3/4}$ is less than the $(\Delta t)_{3/4}$ of low impact velocity. Figure 9 shows the variation of DSIF (K_{ID}) (open symbols) evaluated considering the C_1 term as a function of time. The variation of K_{ID} (dark symbols) with $C_1 = 0$ is also plotted in figure 9. It was observed that the K_{ID} is influenced by the C_1/C_0 ratio and cannot be ignored to estimate the DSIF accurately. At low impact velocity, the crack in epoxy layer propagates with K_{ID} equal to $0.52 \pm 0.04 \text{ MPa}\sqrt{\text{m}}$, close to the fracture toughness of epoxy layer (table 1). The crack in PMMA layer starts propagating with K_{ID} equal to $0.97 \text{ MPa}\sqrt{\text{m}}$, close to the fracture toughness of PMMA layer (table 1). However, it decreases to the value $0.52 \text{ MPa}\sqrt{\text{m}}$, close to the K_{ID} of epoxy layer as the crack propagates in PMMA layer. At high impact velocity, K_{ID} in epoxy layer varies with the gauge location due to spreading of the strain signals. K_{ID} at gauge location 2 is 50% higher than the K_{ID} at gauge location 1 and 3. Crack in PMMA layer propagates with K_{ID} equal to $3.2 \text{ MPa}\sqrt{\text{m}}$, 66% higher than the fracture toughness of PMMA layer.

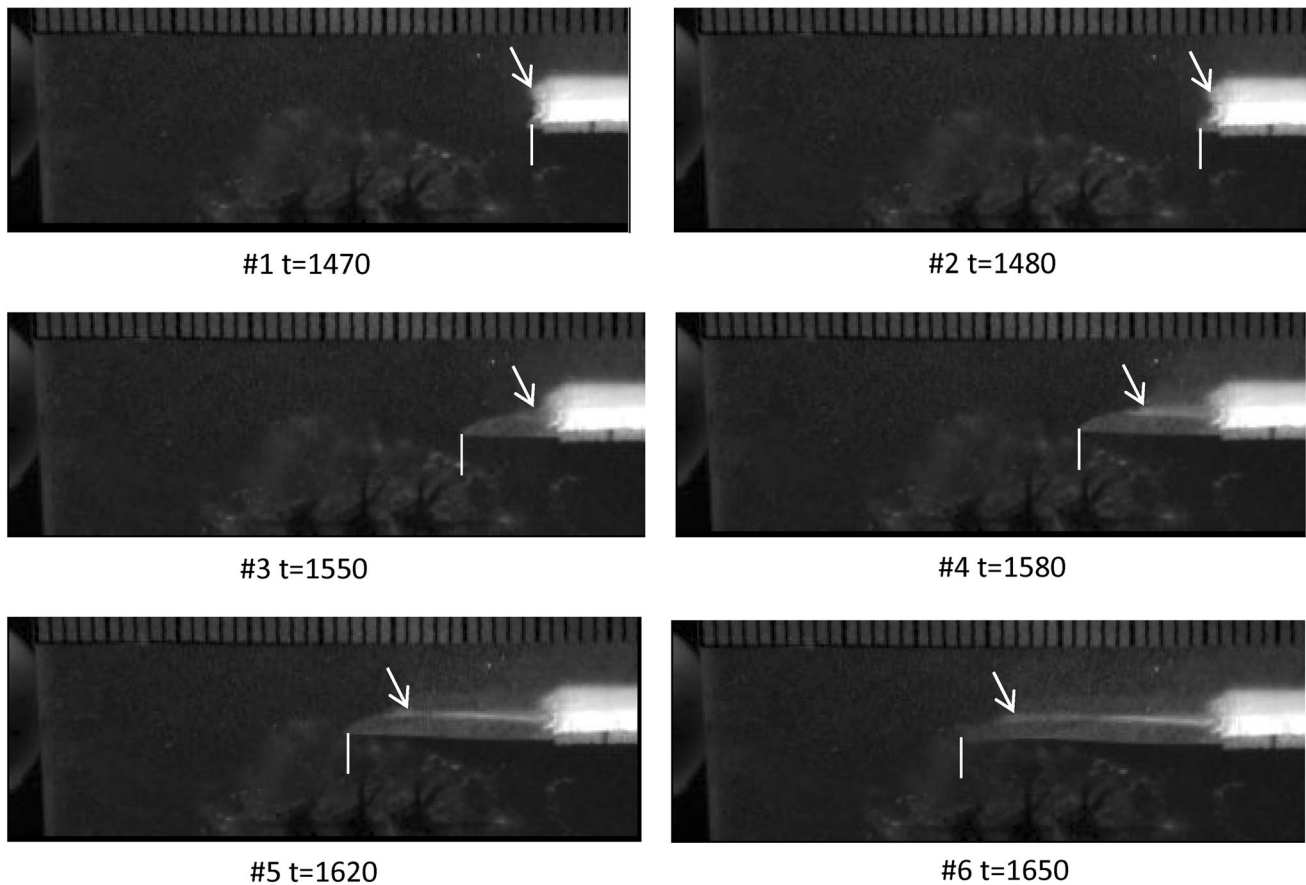


Figure 8. Stages of crack growth in PMMA-Epoxy layered plate ($v = 1.75 \text{ m/s}$).

Table 2. Equivalent time duration and corresponding C_1/C_0 ratio for the epoxy–PMMA layered plate

$v = 1.56 \text{ m/s}$						
	EP			PMMA		
	1	2	3	1	2	3
$(\Delta t)_{3/4}(\mu\text{s})$	53	47	41	44	45	38
C_1/C_0	−46.99	−68.35	−89.79	−79.07	−75.5	−100.51

$v = 5.61 \text{ m/s}$					
	EP			PMMA	
	1	2	3	2	3
$(\Delta t)_{3/4}(\mu\text{s})$	51	34	34	28	27
C_1/C_0	−54.06	−114.8	−114.8	−136.23	−139.81

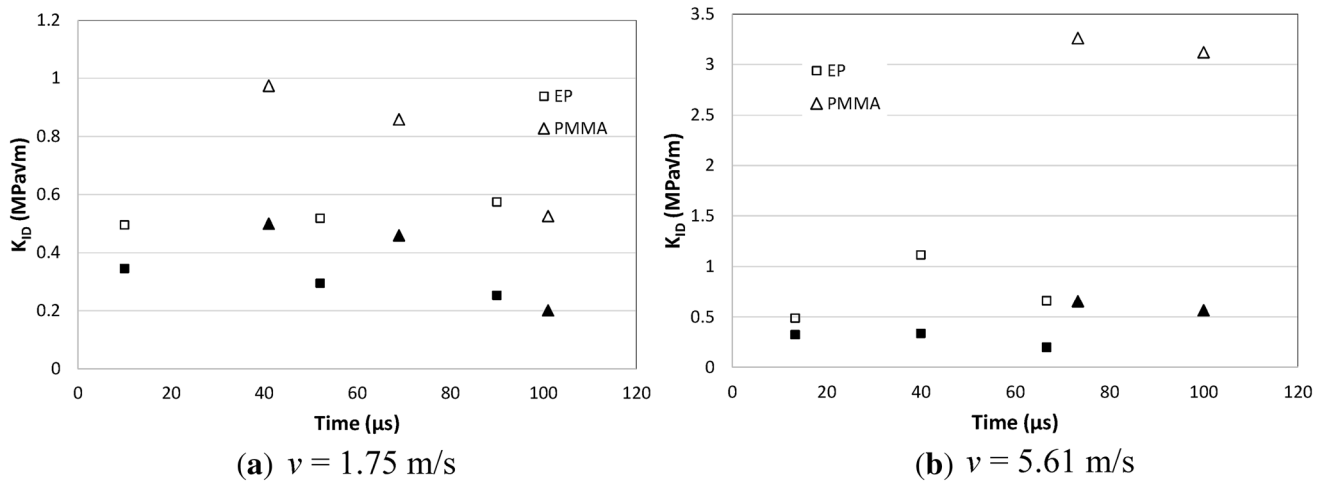


Figure 9. Variation of DSIF with time in E–P plate.

3.2 Evaluation of dynamic SIF of PMMA–epoxy–PMMA (P–E–P) layered plate

In this section, crack initiation and propagation behavior of PMMA–epoxy–PMMA layered plate subjected to an impact velocity of 1.75 m/s will be discussed. Four strain gauges, one at an acute angle and three at an obtuse angle were mounted on the PMMA surface of the specimen. The specimen strain signals obtained from the acute angle and obtuse angle gauge are shown in figure 10. Simultaneously images of the crack growth were also captured at a time interval of 7 μs. Crack lengths when the crack in PMMA layer is just below the strain gauge, were also measured from the images and plotted in figure 10. Similar observations were made as in E–P specimen. The time corresponding to peak strain recorded by acute angle gauge is close to the time at which crack in PMMA layer initiates. The time corresponding to images when crack tip is directly

below the obtuse angle gauges is in good match with the time corresponding to peak strains with an uncertainty of $\pm 7 \mu\text{s}$. The delay in the crack initiation in PMMA layer after the crack extension in epoxy layer was reported as 40 μs. As the epoxy layer is sandwiched between the two PMMA layers, symmetric crack front profile in epoxy layer was observed as shown in figure 11. Vertical line indicates the crack tip in epoxy layer and arrow indicates the crack tip in PMMA layer. Figure 12 shows the crack tip location history in P–E–P plate. Crack in epoxy layer moves with a speed of 50 m/s before the crack initiation in PMMA layer. Once the crack extends in PMMA layer, crack in both epoxy and PMMA layers run with a speed of 123 m/s. As discussed in section 2.2, the equivalent time duration $(\Delta t)_{3/4}$ and corresponding C_1/C_0 ratio are extracted from strain signals and reported in table 3. Figure 13 shows the variation of SIF with time for both acute and obtuse angle

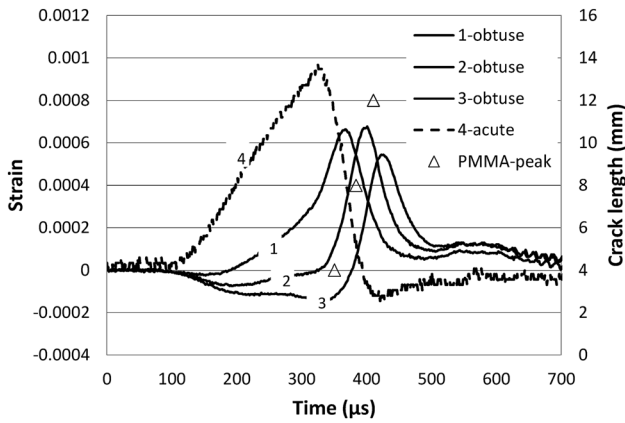


Figure 10. Strain histories in the P-E-P plate during crack propagation at $v = 1.75$ m/s.

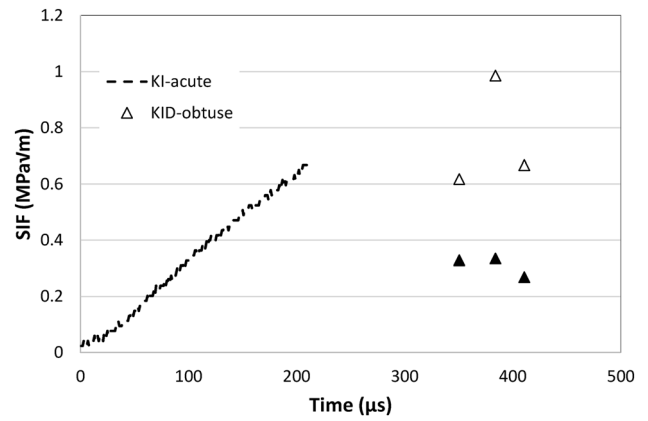


Figure 13. Variation of SIF with time in P-E-P plate.

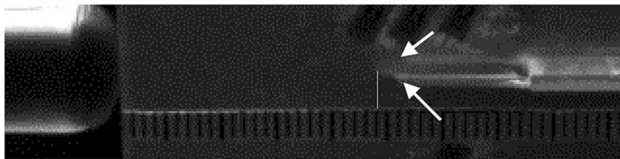


Figure 11. Image during crack growth in P-E-P plate.

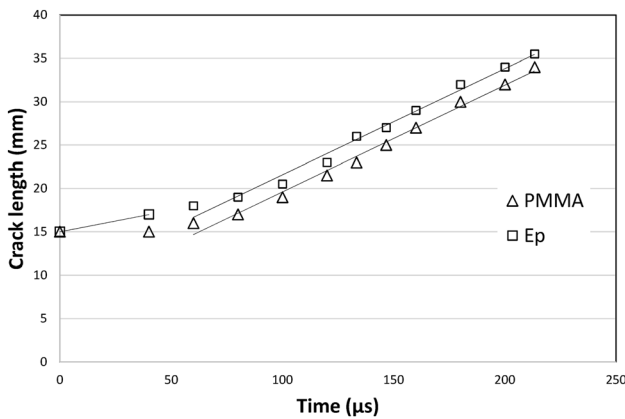


Figure 12. Crack-tip location history in the P-E-P plate at $v = 1.75$ m/s.

Table 3. Equivalent time duration and corresponding C_1/C_0 ratio for the PMMA-epoxy-PMMA layered plate

	$v = 1.56$ m/s		
	1	2	3
$(\Delta t)_{3/4}(\mu s)$	45	36	39
C_1/C_0	-75.5	-107.65	-96.94

orientation. In figure 13, solid filled and open triangle symbols indicate the SIF without considering the effect of C_1 ($C_1 = 0$) and with considering the effect of C_1 respectively. K_I evaluated using acute angle gauge signal varies linearly with time and maximum value of K_I corresponds to the crack initiation toughness of PMMA layer which is lower than the fracture toughness of PMMA layer. K_{ID} evaluated using obtuse angle gauge signal varies with the gauge location. K_{ID} at gauge location 2 is 37% higher than the K_{ID} at gauge location 1 and 2.

4. Summary

In this study, dynamic SIF of an edge cracked layered plates having property jumps across the crack front has been evaluated. Layered structures made of epoxy and PMMA and having same initial crack length were subjected to mode-I dynamic loading. Crack propagation toughness has been estimated by mounting the strain gauges on the specimens at an obtuse angle configuration. A high-speed camera is used to view the crack surfaces in each layer of the layered plates. Experiments were performed on both two-layer and three-layer configuration at different impact velocities. In two-layer configuration, a noticeable delay in crack initiation in PMMA layer after the crack extension in epoxy layer has been found at low impact velocity. However, at high impact velocity the delay has been significantly reduced. While comparing the two-layer and three-layer configuration at the same impact velocity, the delay observed in three-layer configuration is almost half the delay observed in two-layer configuration. This is due to the crack in epoxy layer arrest from both sides by PMMA layer in three-layer configuration. In both layered configuration, two crack speeds were observed in epoxy layer before and after the crack initiation in PMMA layer. Before the crack extension in PMMA layer, the speed of the crack in epoxy layer is slower than the speed after the crack

extension in PMMA layer. It was observed that there are two critical loads, one at which the epoxy layer crack starts extending and the other at which PMMA layer crack starts extending. The critical SIF in epoxy layer at the instant of crack initiation is close to static fracture toughness of epoxy layer. However, the critical SIF in PMMA layer at the instant of crack initiation is slightly lower than the static fracture toughness of PMMA layer. At low and high impact velocities the crack in epoxy layer propagated at critical SIF which is close to the static fracture toughness of epoxy layer. However, in PMMA layer at low impact velocity crack starts propagating with critical SIF close to fracture toughness of PMMA layer and as the crack propagates in PMMA layer, the critical SIF decreases and becomes close to the static fracture toughness of epoxy layer before the final failure of the specimen. At high impact velocity, crack in PMMA layer propagates at critical SIF which is significantly higher than the static fracture toughness of PMMA layer.

Acknowledgements

The author acknowledges the High-Speed Experimental Mechanics Laboratory (HSEML) at IIT Kanpur for performing the experiments. The author is also thankful to Prof. P. Venkitanarayanan for providing the valuable guidance during the experiments. The author acknowledges the financial support of Aeronautical Research and Development Board, India through grant number DARO/08/1051679/M/I. The author also acknowledges the financial support through grant number SR/FST/ERII-003/2006 under the FIST program by Department of Science and Technology, Government of India for the ultra-high-speed camera. The author also thanks Anjani Kumar Varshney for providing MATLAB code for dispersion correction in polymeric bars.

References

- [1] Rice J R and Sih G C 1965 Plane problems of cracks in dissimilar media. *J. Appl. Mech.* 32: 418–423. <https://doi.org/10.1115/1.3625816>.
- [2] Hutchinson J W and Suo Z 1991 Mixed mode cracking in layered materials. In: Wu J W H and T Y, eds. *Adv. Appl. Mech.*, vol. 29, Elsevier; pp. 63–191
- [3] Xu L and Tippur H V 1995 Fracture parameters for interfacial cracks: an experimental-finite element study of crack tip fields and crack initiation toughness. *Int. J. Fract.* 71: 345–363. <https://doi.org/10.1007/BF00037814>.
- [4] Tippur H V and Rosakis A J Quasi-static and dynamic crack growth along bimaterial interfaces: A note on crack-tip field measurements using coherent gradient sensing. *Exp. Mech.* 31: 243–251. <https://doi.org/10.1007/BF02326067>.
- [5] Yang W, Suo Z and Shih C F 1991 Mechanics of dynamic debonding. *Proc. R Soc. Lond. Ser. Math. Phys. Sci.* 433: 679–97. <https://doi.org/10.1098/rspa.1991.0070>.
- [6] Liu C, Lambros J and Rosakis A J 1993 Highly transient elastodynamic crack growth in a bimaterial interface: Higher order asymptotic analysis and optical experiments. *J. Mech. Phys. Solids* 41: 1887–1954. [https://doi.org/10.1016/0022-5096\(93\)90074-P](https://doi.org/10.1016/0022-5096(93)90074-P).
- [7] Singh R P and Shukla A 1996 Subsonic and intersonic crack growth along a bimaterial interface. *J. Appl. Mech.-Trans. ASME - J. APPL. MECH* 63. <https://doi.org/10.1115/1.2787247>.
- [8] Singh R P, Kavaturu M and Shukla A 1997 Initiation, propagation and arrest of an interface crack subjected to controlled stress wave loading. *Int. J. Fract.* 83:291–304. <https://doi.org/10.1023/A:1007358901588>.
- [9] Shukla A and Kavaturu M 1998 Opening-mode dominated crack growth along inclined interfaces: Experimental observations. *Int. J. Solids Struct.* 35: 3961–3975. [https://doi.org/10.1016/S0020-7683\(97\)00193-5](https://doi.org/10.1016/S0020-7683(97)00193-5).
- [10] Shukla A 2001 High-speed fracture studies on bimaterial interfaces using photoelasticity – A review. *J. Strain Anal. Eng. Des.* 36: 119–142. <https://doi.org/10.1243/0309324011512658>.
- [11] Erdogan F and Biricikoglu V 1973 Two bonded half planes with a crack going through the interface. *Int. J. Eng. Sci.* 11: 745–766. [https://doi.org/10.1016/0020-7225\(73\)90004-9](https://doi.org/10.1016/0020-7225(73)90004-9).
- [12] Singh R P and Parameswaran V 2003 An experimental investigation of dynamic crack propagation in a brittle material reinforced with a ductile layer. *Opt. Lasers Eng.* 40: 289–306. [https://doi.org/10.1016/S0143-8166\(02\)00089-1](https://doi.org/10.1016/S0143-8166(02)00089-1).
- [13] Parameswaran V and Shukla A 1998 Dynamic fracture of a functionally gradient material having discrete property variation. *J. Mater. Sci.* 33: 3303–3311. <https://doi.org/10.1023/A:1013277011848>.
- [14] Berger J R, Dally J W and Sanford R J 1990 Determining the dynamic stress intensity factor with strain gauges using a crack tip locating algorithm. *Eng. Fract. Mech.* 36: 145–156.
- [15] Sanford R J and Dally J W 1990 An improved strain gauge method for measuring K_{II} for a propagating crack. *J. Strain Anal. Eng. Des.* 25: 177–183. <https://doi.org/10.1243/03093247V253177>.
- [16] Khanna S K and Shukla A 1995 On the use of strain gauges in dynamic fracture mechanics. *Eng. Fract. Mech.* 51: 933–948.
- [17] Khanna S K and Shukla A 1994 Development of stress field equations and determination of stress intensity factor during dynamic fracture of orthotropic composite materials. *Eng. Fract. Mech.* 47: 345–359. [https://doi.org/10.1016/0013-7944\(94\)90092-2](https://doi.org/10.1016/0013-7944(94)90092-2).
- [18] Ricci V and Shukla A 2003 Subsonic interfacial fracture using strain gauges in isotropic–orthotropic bimaterial. *Theor. Appl. Fract. Mech.* 39: 143–161. [https://doi.org/10.1016/S0167-8442\(02\)00155-6](https://doi.org/10.1016/S0167-8442(02)00155-6).
- [19] Piva A and Viola E 1988 Crack propagation in an orthotropic medium. *Eng. Fract. Mech.* 29: 535–548. [https://doi.org/10.1016/0013-7944\(88\)90179-8](https://doi.org/10.1016/0013-7944(88)90179-8).
- [20] Kuang-Chong W 1991 Explicit crack-tip fields of an extending interface crack in an anisotropic bimaterial. *Int. J. Solids Struct.* 27: 455–66. [https://doi.org/10.1016/0020-7683\(91\)90134-2](https://doi.org/10.1016/0020-7683(91)90134-2).
- [21] Deng X 1992 Complete complex series expansions of near-tip fields for steadily growing interface cracks in dissimilar isotropic materials. *Eng. Fract. Mech.* 42:237–42. [https://doi.org/10.1016/0013-7944\(92\)90214-Y](https://doi.org/10.1016/0013-7944(92)90214-Y).
- [22] Kumar S, Singh IV, Mishra B K and Singh A 2016 New enrichments in XFEM to model dynamic crack response of

- 2-D elastic solids. *Int. J Impact Eng.* 87:198–211. <https://doi.org/10.1016/j.ijimpeng.2015.03.005>.
- [23] Bhardwaj G, Singh IV, Mishra B K and Bui T Q 2015 Numerical simulation of functionally graded cracked plates using NURBS based XIGA under different loads and boundary conditions. *Compos Struct* 126:347–59. <https://doi.org/10.1016/j.compstruct.2015.02.066>.
- [24] Negi A 2019 Localizing gradient damage model with smoothed stress based anisotropic nonlocal interactions. *Eng. Fract. Mech.*;214:21–39. <https://doi.org/10.1016/j.engfracmech.2019.04.011>.
- [25] Mishra R, Burela R and Pathak H 2018 Crack interaction study in piezoelectric materials under thermo-electro-mechanical loading environment. *Int J Mech Mater Des.* <https://doi.org/10.1007/s10999-018-9410-0>.
- [26] Badaliane R and Sih G C 1975 An approximate three-dimensional theory of layered plates containing through thickness cracks. *Eng. Fract. Mech.* 7: 1–22. [https://doi.org/10.1016/0013-7944\(75\)90063-6](https://doi.org/10.1016/0013-7944(75)90063-6).
- [27] Kidane A and Shukla A 2010 Quasi-static and dynamic fracture initiation toughness of Ti/TiB layered functionally graded material under thermo-mechanical loading. *Eng. Fract. Mech.* 77:479–91. <https://doi.org/10.1016/j.engfracmech.2009.10.006>.
- [28] Bankar U H and Parameswaran V 2013 Fracture of edge cracked layered plates subjected to in-plane bending. *Exp Mech*;53:287–98. <https://doi.org/10.1007/s11340-012-9649-6>.
- [29] Agnihotri S K and Parameswaran V 2015 Mixed-mode fracture of layered plates subjected to in-plane bending. *Int. J. Fract.*. <https://doi.org/10.1007/s10704-015-0061-y>.
- [30] Kumar Agnihotri S and Parameswaran V 2016 Dynamic Fracture of Layered Plates Subjected to In-Plane Bending. *J Eng Mater Technol* 138:041016-041016–8. <https://doi.org/10.1115/1.4033911>.
- [31] Shukla A 2006 Dynamic Fracture Mechanics. *World Scientific*.
- [32] Wang L, Labibes K, Azari Z, Pluvinage G 1994 Generalization of split Hopkinson bar technique to use viscoelastic bars. *Int. J. Impact Eng.* 15: 669–686. [https://doi.org/10.1016/0734-743X\(94\)90166-I](https://doi.org/10.1016/0734-743X(94)90166-I).
- [33] Zhao H, Gary G and Klepaczko J R 1997 On the use of a viscoelastic split hopkinson pressure bar. *Int. J Impact Eng.* 19: 319–330. [https://doi.org/10.1016/S0734-743X\(96\)00038-3](https://doi.org/10.1016/S0734-743X(96)00038-3).
- [34] Bacon C 1998 An experimental method for considering dispersion and attenuation in a viscoelastic Hopkinson bar. *Exp. Mech.* 38: 242–249. <https://doi.org/10.1007/BF02410385>.
- [35] Benatar A, Rittel D and Yarin A L 2003 Theoretical and experimental analysis of longitudinal wave propagation in cylindrical viscoelastic rods. *J. Mech. Phys. Solids* 51: 1413–1431. [https://doi.org/10.1016/S0022-5096\(03\)00056-5](https://doi.org/10.1016/S0022-5096(03)00056-5).
- [36] Liu Q and Subhash G 2006 Characterization of viscoelastic properties of polymer bar using iterative deconvolution in the time domain. *Mech. Mater.*38: 1105–1117. <https://doi.org/10.1016/j.mechmat.2006.01.001>.
- [37] Varshney A K 2013 *Testing low impedance materials using a polymeric split hopkinson pressure bar*. M.Tech. thesis, Indian Institute of Technology Kanpur, UP. India